

Richard L. Ehman, MD • Joel P. Felmlee, MS

Adaptive Technique for High-Definition MR Imaging of Moving Structures¹

An adaptive technique for measuring and correcting the effects of patient motion during magnetic resonance image acquisition was developed and tested. A set of algorithms that can reverse the effects of object displacements and phase shifts was used. These algorithms essentially transfer the frame of reference of the image reconstruction from the static frame of the imager couch to the moving "visceral frame." An accurate record of tissue motion during image acquisition is required. To achieve this, the authors used specially encoded "navigator" echoes that are interleaved with the imaging sequence. Postprocessing of the navigator echo data provides a highly detailed record of the displacements and phase shifts that occur during imaging. Phantom studies demonstrated that the technique can directly correct image degradation caused by motion. In contrast to conventional artifact reduction techniques, such as ordered phase encoding and gradient moment nulling, this new method has a unique capacity to reduce motion unsharpness. Preliminary *in vivo* studies have demonstrated that the technique can markedly improve images degraded by voluntary motion and shows promise for addressing the problem of respiratory motion in thoracoabdominal imaging.

Index terms: Magnetic resonance (MR), artifact • Magnetic resonance (MR), image processing • Magnetic resonance (MR), physics • Magnetic resonance (MR), technology, 60.1214, 70.1214

Radiology 1989; 173:255-263

¹ From the Department of Diagnostic Radiology, Mayo Clinic and Foundation, Rochester, MN 55905. From the 1988 RSNA annual meeting. Received February 21, 1989; revision requested May 15; revision received May 22; accepted June 1. R.L.E. is a Du Pont/RSNA Research and Education Fund Scholar. This project also supported by the Mayo Foundation. Address reprint requests to R.L.E.
© RSNA, 1989

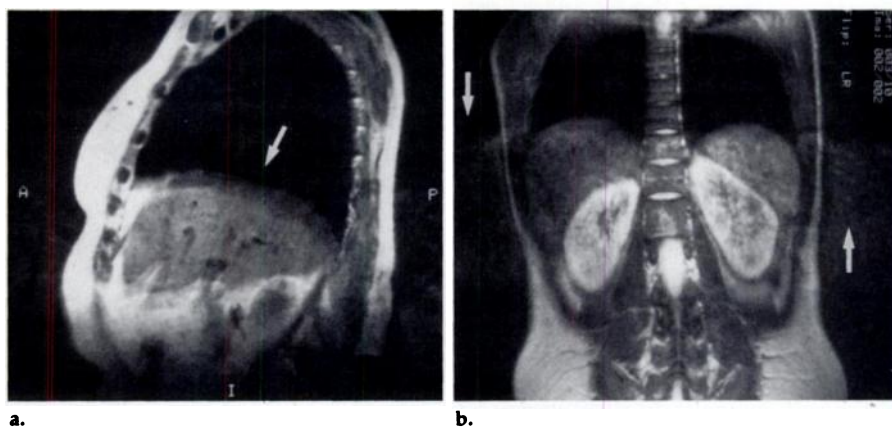


Figure 1. Effects of respiratory motion. (a) Sagittal, short TR/TE image of the thorax and abdomen. Anteroposterior motion of the anterior body wall causes subtle arclike artifacts that are superimposed on the abdominal contents. Much more important is the unsharpness caused by the craniocaudal respiratory motion of the diaphragm and abdominal organs. This is apparent as blurring of the dome of the diaphragm (arrow) and a doubled appearance at the inferior margin of the liver. These effects are due to temporal modulation of the modulus of the transverse magnetization as tissues move from voxel to voxel. (b) Coronal T2-weighted image of a different patient. Respiratory craniocaudal motion of the liver and spleen causes displaced ghost images of these organs, which are apparent on both sides of the abdomen (arrows). These effects are due to temporal modulation of the phase of the transverse magnetization of volume elements.

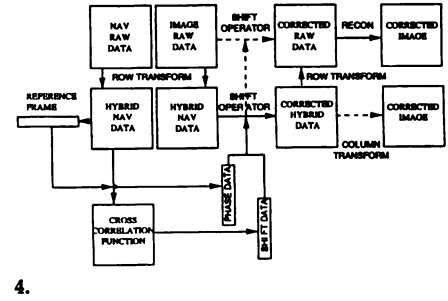
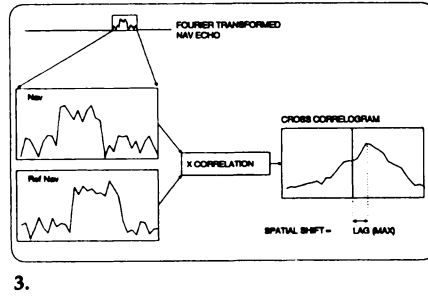
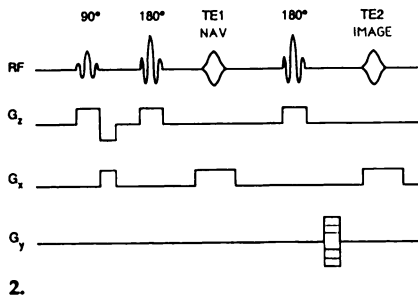
PHYSIOLOGY dictates that many structures of clinical interest in magnetic resonance (MR) imaging are in a natural state of motion. This factor has assumed increasing importance in the past several years, as technical developments have improved the signal-to-noise ratio of MR imaging systems to such a point that physiologic motion is the most important remaining limitation in many examinations.

Motion has complex effects on the spin-warp (two-dimensional Fourier transform) MR imaging process, causing artifacts, intensity loss, and unsharpness (1-5) (Fig 1). These processes decrease the clarity with which lesions and anatomic details can be depicted. The components of patient motion include so-called physiologic motion (vascular, cardiac, gastrointestinal, and respiratory) and gross movements that may be voluntary or involuntary.

Methods for fast acquisition of MR images (gradient-recalled and echo-planar techniques) hold great promise for reducing the effects of motion (6-10). Nevertheless, these techniques have limitations such as reduced signal-to-noise ratio, vulnerability to certain artifacts, and unproved contrast characteristics. To our knowledge, the extent to which these techniques can replace spin-echo imaging in clinical practice has not yet been established.

A variety of other techniques for reducing motion degradation in MR images have been introduced in the past several years, including physiologic gating, ordered phase encoding, gradient moment nulling, and presaturation (11-17). Each technique has specific capabilities and limita-

Abbreviations: NAV = navigator, TE = echo time, TR = repetition time.



Figures 2-4. (2) NAV sequence. G_x = x-axis gradient, G_y = y-axis gradient, G_z = z-axis gradient, RF = radio frequency. (3) Method of processing NAV echoes. (4) Overview of data processing strategy.

tions. Electrocardiographic gating has been successful for cardiac and spinal imaging. While respiratory gating has been shown to decrease artifacts and unsharpness in thoracoabdominal MR images, it has not been widely adopted because of its time penalty. Ordered phase encoding (respiratory compensation), gradient moment nulling (flow compensation), and presaturation can be used separately or in combination to reduce a variety of motion artifacts, but these techniques share an important limitation: They have little capacity to reduce motion unsharpness. In addition, none of the aforementioned techniques can address the problem of voluntary or involuntary gross patient movement during image acquisition.

During MR image acquisition, motion causes changes in the position of structures in the field of view from one phase-encoding measurement to another. We call these *view-to-view* changes. Similarly, during the process of measuring a single phase-encoding view, moving tissue and flowing blood can cause variable phase shifts. We call these *intraview* effects. While the temporal pattern of these effects is unique to each data acquisition, the physical continuity of tissue ensures that many of the important motions are global in nature and similarly affect many volume elements within a given field of view. This is in contrast to the characteristics of fluid motion, in which shear has a substantial influence. With normal tidal breathing, for instance, the liver, kidneys, and spleen collectively move craniocaudally a distance of approximately 2 cm (18).

These considerations have led us to investigate the possibility of using mathematical techniques to adaptively correct raw image data for global view-to-view motion and for bulk phase shifts caused by variable intraview tissue motion. These mathematical operations effectively lock the frame of reference of the reconstruc-

tion onto the moving "visceral frame" rather than the static frame of the imager couch. The technique requires detailed information about the motion of the objects of interest during image data acquisition. We postulate that such information can be extracted from special "navigator" echoes that are interleaved with the normal echoes used for imaging.

The purpose of this study was to investigate the feasibility and potential of these adaptive correction techniques.

METHODS

The separate tasks of correction and measurement are described individually in this section, and assumptions and limitations are addressed in the Discussion section.

Algorithms for Correction of Object Displacements and Motion-induced Phase Shifts

Appendix A provides a short intuitive derivation of a set of mathematical operations that can correct MR imaging data for view-to-view displacements of an object in the x, y, and z directions (x and y only with two-dimensional Fourier transform imaging) and also for phase shifts due to intraview motion in any direction. The algorithm shifts the apparent distribution of spins in each successive spin echo to compensate for view-to-view displacements and applies a phase rotation that is opposite to the observed phase perturbation due to intraview motion. All of these corrections can be implemented by appropriate phase rotation of the quadrature signal intensity measurements in the raw data set. The following equation represents the unique corrective phase shift $\Delta\phi_c(j,k)$ that would be applied to the j th sample of an echo comprising the k th phase-encoding view of a two-dimensional Fourier transform raw data set:

$$\Delta\phi_c(j,k) = \Delta\phi_x + \Delta\phi_y + \Delta\phi_p, \quad (1)$$

where $\Delta\phi_x$, $\Delta\phi_y$, and $\Delta\phi_p$ are defined in Appendix A and depend on motion along the x and y directions. In general, each of these terms depends on the sample number (j) and view number (k).

Methods for Measuring and Recording Object Displacements and Phase Shifts

The adaptive corrections described in the previous section require detailed information about the position of an imaged object and its phase shift due to intraview motion at the time of each echo. A variety of approaches might be possible, but we have evaluated the use of specially encoded echoes that can be interleaved into the imaging sequence. These echoes are designed to permit accurate tracking of the position and phase of an object of interest within the field of view and will henceforth be referred to as navigator (NAV) echoes. Other investigators have proposed the use of a similar interleaved echo, but only for gating purposes and not as part of an adaptive correction system (19).

Measurement of view-to-view displacement.—Figure 2 illustrates a prototype NAV echo sequence designed to provide x-axis displacement information. The NAV echo is similar to an image echo, except that no phase encoding is applied. This implies that the NAV echo data will vary from view to view only if motion along the x axis is present. The order of the echoes could be reversed if desired. In that case, phase encoding would be applied before the first (image) echo and then would be "unwound" by an additional y-axis gradient before the NAV echo.

Figure 3 illustrates an approach for the processing of successive NAV echoes in such a way that the x-axis (X-NAV) displacements of a moving object can be determined with respect to a reference view. The X-NAV echoes are Fourier transformed into projections in hybrid space, and modulus values are calculated. A single NAV projection is arbitrarily chosen as a reference, and cross-correlation functions are calculated with respect to each of the other NAV projections. The abscissa corresponding to the maximum value in each cross-correlation function is then a measure of the x displacement (in pixels) of the object, with respect to the reference NAV view. This assumes that the motion is not so rapid that a significant displacement would occur in the short time (10–20 msec) between the NAV and the image echoes. It may be desirable to use the first echo for imaging and the second for NAV information in

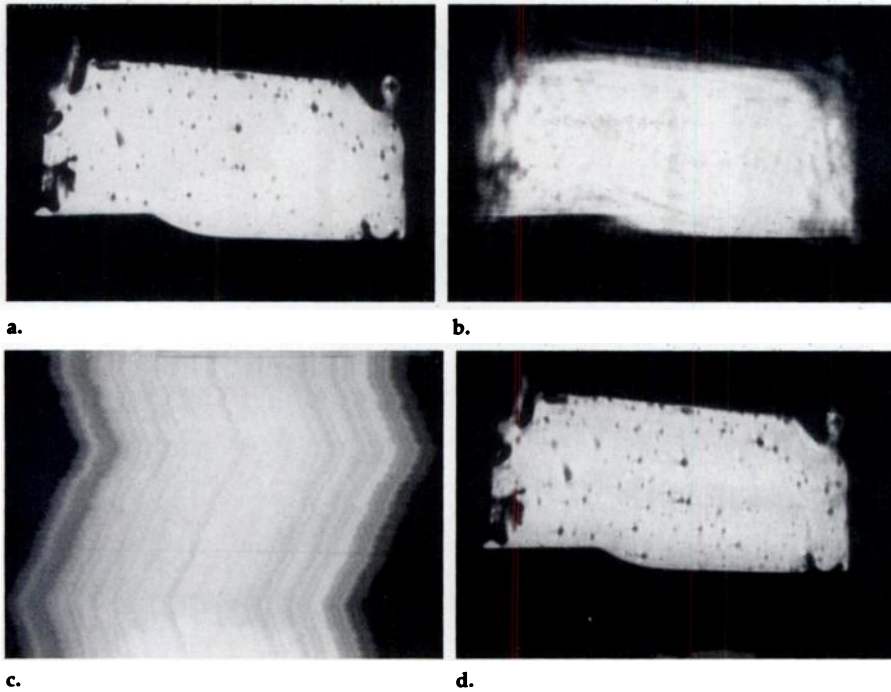


Figure 5. Adaptive correction of view-to-view displacement. (a) Image shows the appearance of the phantom in a motionless state. (b) Uncorrected image obtained with the X-NAV sequence when the phantom was manually moved from side to side (x direction) during acquisition at low velocities of less than approximately 1 cm/sec. Note the total loss of internal detail due to motion unsharpness and the presence of motion artifacts. (c) Image shows a portion of the X-NAV data obtained during the same acquisition. These echoes have been Fourier transformed, and their modulus is displayed in order of acquisition from top to bottom. Each horizontal raster line illustrates the transverse position of the phantom at the time the NAV echo was collected. (d) The X-NAV data were processed to determine the displacement of the phantom from a reference position at each time in the acquisition. With these data, the adaptive algorithm was applied to the same raw data used to make the image in b. The corrected raw data were reconstructed to yield the image in d. The correction technique has achieved the desired objective of correcting both artifacts and unsharpness.

sequences with short repetition times (TRs) and echo times (TEs). Other variations could use gradient echoes for NAV purposes rather than spin echoes to minimize cycle time or to avoid sacrificing an imaging echo.

Displacement along the y axis could be similarly obtained by applying the readout gradient of the NAV echo along the y axis (Y-NAV) rather than along x. A combined XY-NAV sequence could incorporate an X-NAV echo before the image echo and a Y-NAV echo after it. The idea could be extended to three dimensions by adding a NAV echo along the z axis as well. It is also possible to derive both x and y displacement information from a single NAV echo sequence if a small amount of constant phase encoding is applied to an X-NAV echo. In this case, displacements in the x direction are determined by cross correlation in hybrid space as already described. Displacements in the y direction are detected as phase shifts that are proportional to the magnitude of y displacement and the total phase twist applied across the field of view by the constant y gradient.

Measurement of phase shifts due to intraview motion.—Consider the X-NAV sequence illustrated in Figure 2. If intraview

motion (along any axis) causes a bulk phase shift, it will be detectable in the hybrid NAV data in the segment in which the modulus of the object is concentrated. The phase shift due to intraview motion can be determined for each NAV echo by calculating the phase angle of complex (I, Q) data points at appropriate locations in each NAV projection in hybrid space and then subtracting corresponding phase angles from a NAV projection obtained when the object is static.

With a few caveats, the motion-induced phase shifts observed in each NAV echo are proportional to the phase shifts present in the corresponding image echoes. Among other things, this assumes that the velocity of the object does not change significantly in the time between the NAV echo and the image echo. If the proportionality constant can be determined with calculation or calibration, then the image echo data can be adaptively corrected for intraview motion with the algorithm outlined in the previous section.

Phantom Studies

The NAV echo sequence illustrated in Figure 2 was implemented on a 1.5-T imager (GE Medical Systems, Milwau-

kee). A variety of phantom studies were performed in the course of developing the adaptive correction technique. Pertinent examples will be described in this section.

A plastic bladder was filled with ultrasound gel to serve as a motion phantom. The irregular margins of the phantom and suspended air bubbles provided detail for assessing the effectiveness of the motion correction techniques. In the initial feasibility studies, the phantom was imaged transversely while it was reciprocating at varying rates and amplitudes in the frequency-encoding direction during acquisition. The field of view was 24 cm and the section thickness was 0.5 cm. All imaging was performed with 256 phase-encoding views and two signal acquisitions. The TR and TE values varied, depending on the purpose of the experiment. The general scheme of data processing is illustrated in Figure 4. In all studies, the second view in the data set was arbitrarily selected as the reference frame.

A phantom with a circular cross section was filled with mineral oil and used to test the hypothesis that a single NAV echo could be used to monitor both the x and y displacements of an object, as described in Appendix A. The NAV sequence was modified to include an extra gradient just before the NAV echo, which imparted a fixed phase rotation across the field of view in the y direction (6π radians in these studies). Imaging was performed with a 24-cm field of view, 5-mm section thickness, 256 views, two signal averages, a TR of 400 msec, a NAV TE of 20 msec, and an image TE of 40 msec. Arbitrary motion in the xy plane was manually imparted during image acquisition. The processing of the NAV data was similar to that shown in Figure 4, except the observed phase shifts were converted to y displacement data (Appendix A).

In Vivo Studies

Preliminary in vivo studies were performed with the pulse sequence illustrated in Figure 2. All studies were performed with 256 views and two signal averages. Fields of view, section thickness, TR, and TE were selected according to the purpose of each study.

In the first in vivo experiments, we evaluated the capacity of the technique to correct spontaneous voluntary motion of an extremity during image acquisition. In the example to be illustrated, the volunteer was asked to spontaneously shift one leg from side to side by approximately 2 cm during acquisition, while the other extremity was fixed in place.

The NAV echo sequence was used to image the abdomen of volunteers to assess the usefulness of this approach for measuring respiratory movements. To provide a preliminary assessment of the potential of the adaptive correction algorithm for abdominal imaging, we applied a correction for displacement to one of the studies.

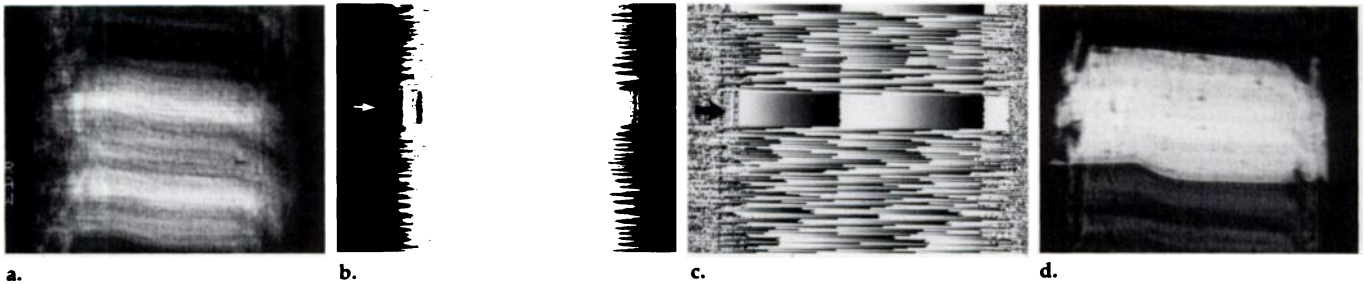


Figure 6. Combined displacement and phase shift correction. (a) Uncorrected image in which the phantom was shifted much more vigorously during acquisition. (b) Image shows the modulus of the transformed X-NAV echoes obtained during a portion of the acquisition. Note that although the rate of motion was generally high, there was a brief pause in the motion (arrow). (c) Image shows the phase of the same group of X-NAV projections. During the pause when the phantom was static (arrow), the phase of successive X-NAV projections was identical at corresponding x-axis locations from line to line. During vigorous motion, however, the phase along a vertical column of points varies from projection to projection. This is due to the effects of intraview motion. (d) The displacement and phase shift data extracted from the NAV echoes were used to correct the raw image data. These data were reconstructed to yield the image in d, which is substantially improved in comparison with the original in a. The residual artifact in d is largely due to aliasing of the phase shifts in the NAV data, a problem that can be corrected by adjusting the TE of the NAV echo.

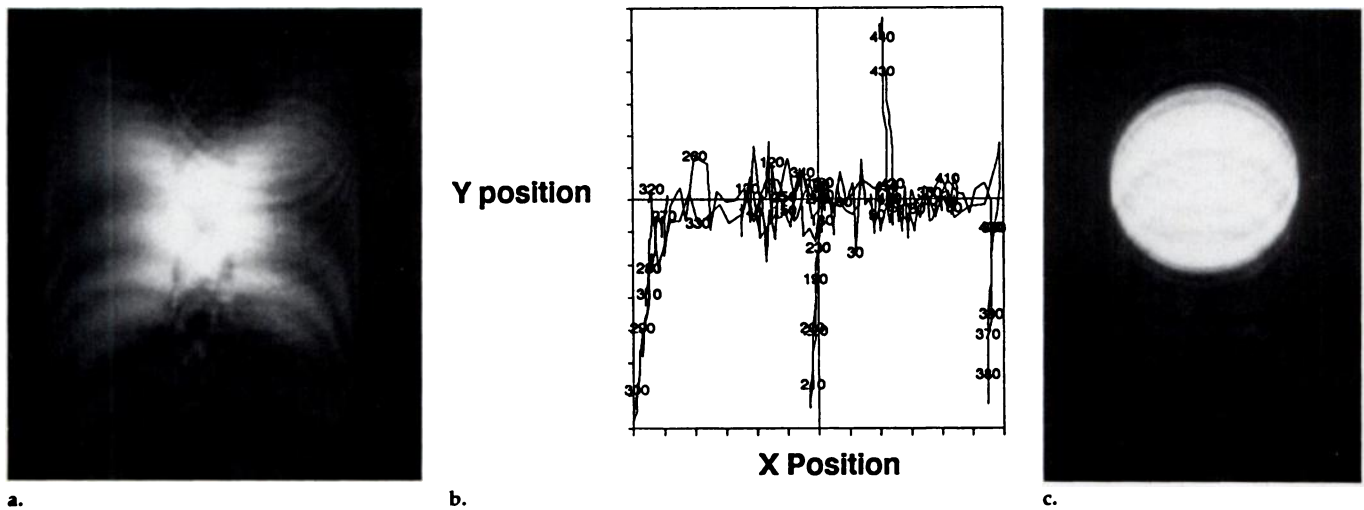


Figure 7. Two-dimensional displacement monitoring and correction. A cylindrical phantom filled with mineral oil was shifted slowly in the xy plane during image acquisition. The NAV echo sequence was modified to provide two-dimensional localization information from the single NAV echo. (a) Uncorrected image shows that the circular cross section of the phantom is completely lost due to motion. The NAV echo data were processed to extract the x and y coordinates of the object during image acquisition. The calculated trajectory of the object in the xy plane is shown schematically in b. The numbers along the course of the trajectory refer to the order of acquisition of NAV echoes, from 1 to 512. These data were used to correct for x and y displacements in the raw image data. (c) Reconstructed corrected image depicts the phantom much more clearly.

RESULTS

Phantom Studies

The phantom studies provide strong support for the adaptive correction concept. The experiment shown in Figure 5 was designed to test the capacity of the adaptive correction method to correct data sets in which the motion effects are primarily due to view-to-view displacements. Accordingly, the phantom was shifted relatively slowly, so that phase shifts due to intraview motion would be minimized. The TR was 400 msec, the NAV TE was 30 msec, and the image TE was 70 msec in this case. The modulus NAV data provided a clear record of the transverse po-

sition of the phantom during imaging. The corrected image in Figure 5d is almost indistinguishable from the static image in Figure 5a.

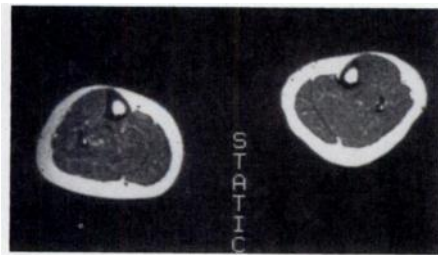
Figure 6 illustrates an experiment in which the phantom was moved more rapidly (up to approximately 5 cm/sec), thereby increasing the influence of intraview motion on the spin-echo data. The influence of intraview motion is well shown in the phase map of the NAV echoes (Fig 6c). When corrections for either view-to-view or intraview motion were applied individually to the MR data set, little benefit was achieved. Figure 6d demonstrates the effectiveness of the technique when both methods are combined.

Further phantom studies have ver-

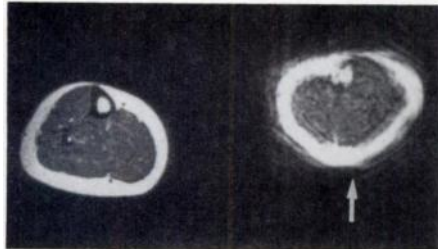
ified the algorithms for correction of motion in the phase-encoding direction. Figure 7 illustrates a two-dimensional correction for both x and y displacements during imaging, with x and y displacement data derived from a single NAV echo (Appendix A). Phase shifts due to intraview motion lead to error in the estimation of y position during imaging, factors causing residual artifacts in the corrected image. However, the corrected image is clearly improved, compared with the uncorrected image.

In Vivo Studies

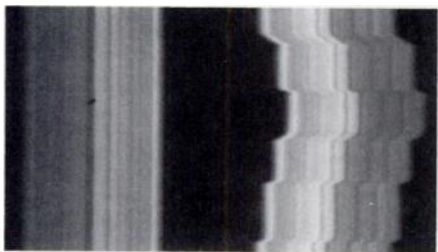
Figure 8 shows an example of one of the studies of the extremities. The NAV echo display clearly demon-



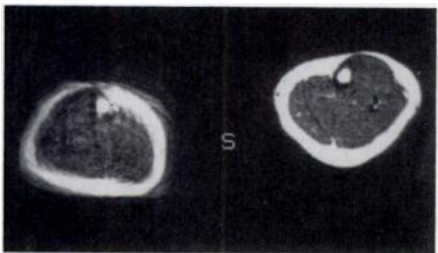
a.



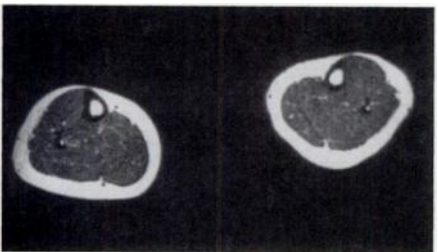
b.



c.



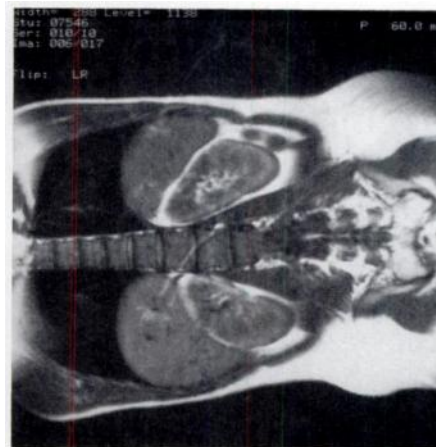
d.



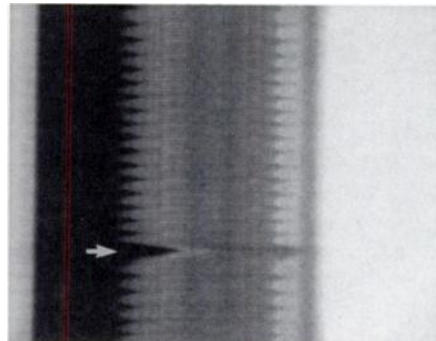
e.

Figure 8. In vivo regional correction of voluntary motion. (a) Image shows a transverse section of the static legs of a volunteer. (b) A second acquisition shows that the left leg was moved spontaneously from side to side and the right leg was stationary. Note the artifacts and unsharpness caused by the leg motion (arrow). (c) Image shows the modulus X-NAV data obtained during the acquisition. The temporal pattern of motion of the left leg and the constant position of the right leg are clearly shown. (d) Image was obtained by applying a global adaptive correction to the raw data. X-displacement information for the left leg was provided by NAV echo data. The image of the left leg has been markedly improved and is almost equal to the static image. As expected, the image of the right leg is now degraded by "pseudomotion" imparted by the correction process. (e) Image was obtained by using a regional correction. The effects of the motion of the left leg are eliminated while the right leg is still depicted clearly.

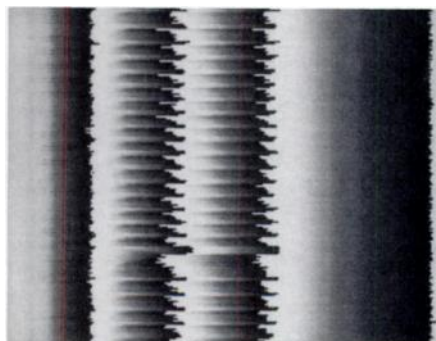
strates the lateral movements during imaging. In processing the NAV data, it was necessary to exclude the segment of each NAV projection spanning the static leg, since this would otherwise reduce the accuracy of the position determination for the moving leg. The segment for exclusion can be identified by computing the variance of each column in the NAV data array. This also provides a template for selectively applying the



a.



b.



c.

Figure 9. In vivo tracking of diaphragm motion with NAV echoes. (a) Uncorrected coronal spin-echo image of the abdomen, obtained with a TR of 500 msec, shows the right and left hemidiaphragm, liver, spleen, and kidneys. The frequency-encoding (x) axis is oriented longitudinally in this acquisition. (b) Image shows the modulus of transformed X-NAV echoes. Note the wave-like pattern at interface between the low intensity of the thorax and the higher intensity of the abdomen, which reflects the craniocaudal motion of normal, quiet tidal breathing (excursions of approximately 2.5 cm in this subject). The larger diaphragm movement (arrow) of approximately 6 cm is a sighing respiration that periodically appears in normal, quiet breathing patterns. (c) Phase display of the transformed X-NAV echoes shows the cyclical phase shifts caused by intraview motion and the slightly larger and more prolonged phase disturbance caused by the sighing respiration. This example provides evidence for the feasibility of measuring respiratory movements simultaneously with image acquisition.

a coronal image of the abdomen obtained with the NAV echo sequence. The most important observation is that the corrected image depicts structures that are not evident at all in the conventional image.

DISCUSSION

The results demonstrate that the adaptive correction technique is capable of directly addressing many of the effects of motion in MR images. In contrast to other techniques, which only reduce artifacts, the method has a unique capability to reduce motion unsharpness. There are few practical penalties associated with the use of the NAV sequence. There is no increase in imaging time. On the basis of the implementation of the NAV echo, there may be a modest reduction in the total number of sections that can be acquired.

The technique shows particular promise for correcting gross motion. Voluntary motion can be a major im-

correction to the image data in hybrid space to yield the regionally corrected image in Figure 8e.

The ability of the NAV technique to track visceral motion is illustrated in Figure 9.

In Figure 10, a correction for view-to-view displacements was applied to

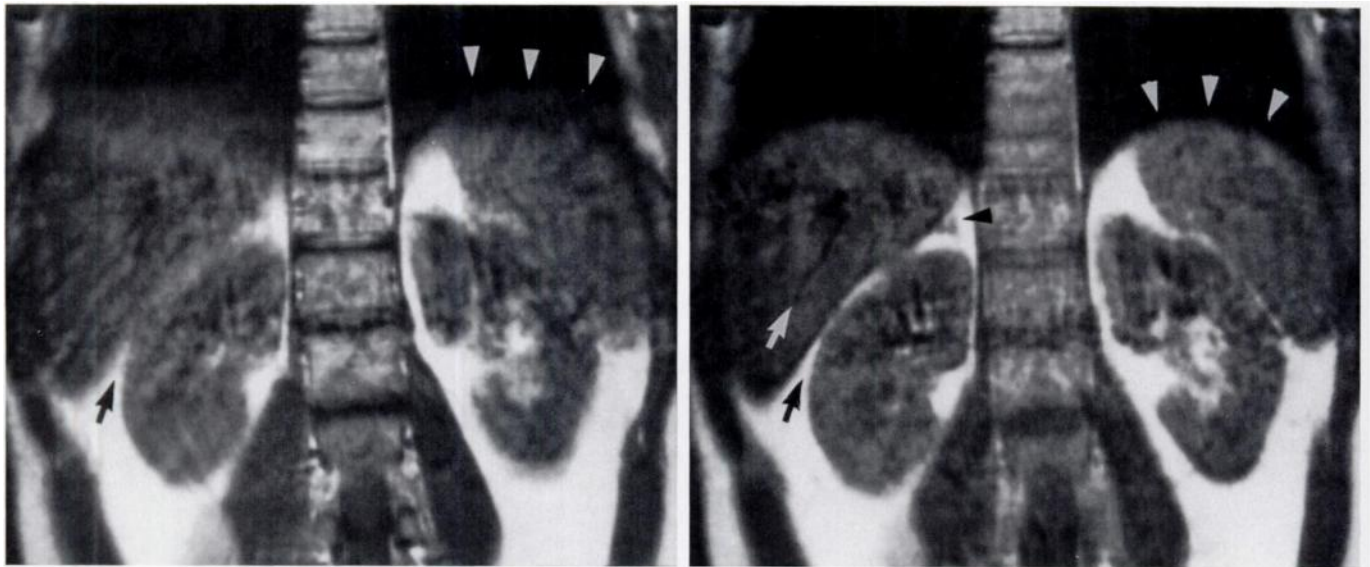


Figure 10. Adaptive correction of respiratory motion. (a) Uncorrected coronal image (TR of 400 msec, TE of 40 msec) of the abdomen of a volunteer, obtained with 256 views, two signal averages, and a section thickness of 5 mm. Sequence included a NAV echo with a TE of 20 msec. The unsharpness of the diaphragm caused by craniocaudal respiratory motion is readily appreciated (arrowheads). Similar unsharpness is apparent at the upper and lower poles of the kidneys and in the poor definition of the fat plane between the liver and the right kidney (arrow). (b) Information from the NAV echo data has been used to correct the data for view-to-view displacements in the craniocaudal direction. Note that the contour of the diaphragm (white arrowheads) is much sharper in this image than in the uncorrected image. Similarly, the upper and lower poles of the kidneys are more clearly defined, and the fat plane between the liver and right kidney is much sharper (black arrow). Most important, intrahepatic vascular structures (white arrow) and the right adrenal gland (black arrowhead) are visible in the corrected image, whereas they were essentially invisible without the adaptive correction technique.

pediment in MR studies of any part of the body—especially in examinations of uncomfortable, disoriented, and seriously ill patients. A single shift of position during a long acquisition can markedly degrade all of the reconstructed images. Pediatric examinations can be especially problematic in this regard, since sedation or even general anesthesia is often required. In many cases the proposed technique should have the capacity to correct images that have been degraded by such motion.

The mode of adaptive correction is entirely independent of other currently available techniques. This method could be combined with other artifact reduction techniques such as gradient moment nulling, ordered phase encoding, or presaturation.

An obvious limitation of the technique is that it cannot correct for view-to-view z-axis displacement in conventional two-dimensional Fourier transform transaxial images. Nevertheless, it can correct for phase shifts due to z-axis intraview motion in such images, and it should be applicable to displacement in any direction in three-dimensional Fourier transform acquisitions. Important issues also arise from the inherent assumption that only a single globally moving object is present within the

field of view. These are addressed in Appendix B.

The results are sufficiently encouraging to warrant further investigation, and several directions are apparent. If the technique can be perfected, it could provide images of thoracoabdominal structures that are less affected by the 2-cm craniocaudal excursion of respiration.

There are interesting parallels and differences between the correction technique for intraview motion described here and gradient moment nulling. Both techniques will correct phase shifts due to bulk motion of solid tissue, but in contrast to gradient moment nulling, the adaptive method specifically “refocuses” only the selected tissues. This may permit the selective enhancement of specific structures in images on the basis of their unique motions, while the detail of surrounding tissues is suppressed. The method offers interesting possibilities for quantitatively measuring or characterizing the physiologic motions of tissue structures with MR imaging.

We speculate that the adaptive correction technique may be suitable for removing the effects of respiratory motion unsharpness from MR angiograms, especially in the potential application of coronary artery imaging.

APPENDIX A

Algorithms for Adaptive Correction of Effects of Object Motion

The raw MR imaging data collected in a spin-warp acquisition can be ordered in an array with rows corresponding to individual phase-encoded spin echoes. This array can be regarded as a map of spatial frequencies, and we will refer to this plane as “data space.” In a typical reconstruction scheme, each of the rows in the data array are Fourier transformed to yield an intermediate array. Each of the columns of the intermediate array are then Fourier transformed to yield a final complex image array. The intermediate array has spatial coordinates in the x direction and spatial frequency coordinates in the y direction, so that this plane is sometimes called “hybrid space.”

The effects of displacement (view-to-view motion) and phase shift (intraview motion) are separated in this discussion, and, for simplicity, we will focus on the case of a single moving object within the field of view.

A typical raw MR imaging data set might consist of an array of 256×256 complex numbers. Each horizontal line of complex points in the array is a digitized spin-echo signal. The digitized values are complex because conventional MR imagers have detection circuitry that yields in-phase (*I*) and quadrature (*Q*) signal voltages that are sampled to give a pair of data values at each point in time.

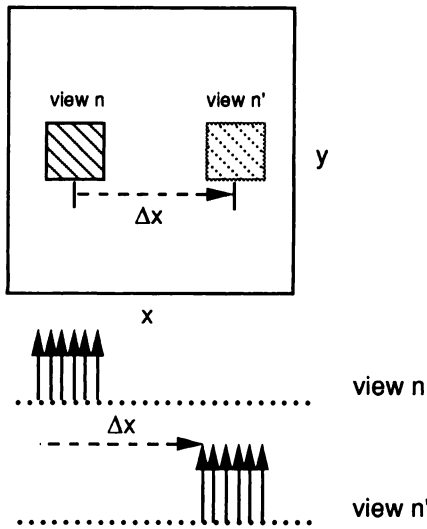


Figure A1. Displacement in the x direction.

The successive lines of spin-echo data in the array are obtained with different phase-encoding gradient amplitudes, which are typically stepped through 256 different values during imaging.

View-to-view displacements in the x (frequency-encoding) direction.—Consider a single small object that moves from position (x,y) to position $(x - \Delta x, y)$ in the time between acquisition of two spin-echo signals (Fig A1). If both spin echoes were acquired with the same phase encoding, then the only difference between them is due to the displacement in the frequency-encoding direction. The difference is best appreciated by examining these data after they have been Fourier transformed:

$$\tilde{S}_{jk}(\text{data space}) \rightarrow \tilde{S}_{jk}(\text{hybrid space}), \quad (\text{A1})$$

$$\tilde{S}_{jk} = \frac{1}{256} \sum_{j=0}^{255} \tilde{S}_{jk} e^{\frac{i2\pi jx}{256}}, \quad (\text{A2})$$

where j is an index for 256 samples of a spin echo. The x axis in hybrid space corresponds directly to the x axis in image space. The effect of an object displacement by $-\Delta x$ is to shift the I, Q values in hybrid space by a distance of $-\Delta x$. This suggests that a particular spin-echo view can be corrected for a known arbitrary displacement $-\Delta x$ simply by Fourier transforming the data, shifting the data by $+\Delta x$, and then inverse Fourier transforming back into data space. Alternatively, the line of hybrid data could simply be stored in preparation for a column transform to create an image.

The Fourier shift theorem (20) provides a way to implement this correction directly in data space. It states that if $f(x)$ has the Fourier transform $F(j)$, then $f(x - \Delta x)$ has the Fourier transform $e^{-i2\pi\Delta x j} F(j)$. This constitutes a phase rotation of each complex point in the sampled spin echo. When the use of discrete transforms is considered, the phase rotation in the j th sample caused by a displacement of Δx pixels would be

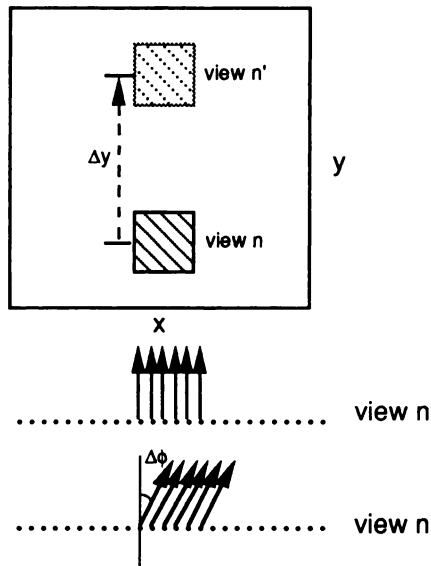


Figure A2. Displacement in the y direction.

$$\Delta\phi_x = \frac{2\pi\Delta x j}{N_x}, \quad j = 0 \text{ to } N_x - 1, \quad (\text{A3})$$

where N_x is the total number of samples of the spin-echo signal. The maximum rotation would be reduced by using the center of the sampled echo as the zero point and rotating the earlier points negatively:

$$\Delta\phi_x = 2\pi\Delta x \left[j - \left(\frac{N_x - 1}{2} \right) \right] \frac{1}{N_x}. \quad (\text{A4})$$

If the position of an object moving arbitrarily in the x direction is accurately known relative to some reference position, this equation provides a method for adaptively correcting each digitized spin echo. When a two-dimensional Fourier transform reconstruction is performed on a corrected data set, the final image should appear as if the object were static at the reference position.

The phase rotation can be implemented with the following formulas:

$$I' = I \cos(\Delta\phi) - Q \sin(\Delta\phi), \quad (\text{A5})$$

$$Q' = I \sin(\Delta\phi) + Q \cos(\Delta\phi), \quad (\text{A6})$$

where I and Q are the original values and I' and Q' are the corrected values.

View-to-view displacements in y (phase-encoding) direction.—Consider a single small object that moves a distance Δy along the y axis in the time between two spin echoes with identical phase encoding (Fig A2). The modulus M_{xy} of complex numbers in raw data space, hybrid space, or image space is defined as

$$M_{xy} = \sqrt{I^2 + Q^2}. \quad (\text{A7})$$

M_{xy} is simply the length of the vector represented by the complex number (I, Q) . While there is no difference in the modulus of the two spin echoes in hybrid space, there is a well-defined phase difference due to the application of phase encoding. For a given phase-encoding

view k , ranging from 0 to $N_y - 1$, the total phase twist across the field of view in the y direction is

$$\Delta\phi_y = 2\pi \left[k - \left(\frac{N_y - 1}{2} \right) \right]. \quad (\text{A8})$$

The phase difference caused by a displacement of Δy pixels in the y direction is then

$$\Delta\phi_y = 2\pi\Delta y \left[k - \left(\frac{N_y - 1}{2} \right) \right] \frac{1}{N_y}. \quad (\text{A9})$$

To correct a spin echo for such a y displacement, it is simply necessary to rotate each I, Q vector in hybrid space by the reverse of this phase angle. By a corollary of the Fourier addition theorem (20), this phase rotation can be applied to all of the points in the digitized spin echo in data space, with the same result.

View-to-view displacements in the z direction.—In the case of section-selective two-dimensional Fourier transform imaging, it is not possible to adaptively correct raw data in retrospect for view-to-view displacements in the logical z direction. Such motions could be corrected if a three-dimensional Fourier transform imaging process were used, because the z -axis motion would be along either a frequency- or phase-encoding axis. On the assumption of the latter, the phase rotation for a three-dimensional Fourier transform acquisition would be

$$\Delta\phi_z = 2\pi\Delta z \left[l - \left(\frac{N_z - 1}{2} \right) \right] \frac{1}{N_z}, \quad (\text{A10})$$

where Δz is the pixel displacement along z , l is the z view number, and N_z is the total number of resolvable elements in that direction. Again, this phase rotation can be applied in data space or hybrid space.

Bulk phase shifts due to intraview motion in the x, y, or z directions.—Consider a single uniform object that moves at a given velocity during the time TE of a spin-echo acquisition. We will compare the spin-echo signal obtained from this moving object to the signal that would be derived from a static object located at the same position at the time TE . To a first approximation, the differences in the spin-echo signals will be purely due to phase shifts of the transverse magnetization M_{xy} . The magnitude of the phase shift is dependent on the direction of motion with respect to the x , y , and z axes; the gradients applied in these directions; and the time derivatives of the motion (21–26). Regardless of the origin of the phase shifts or the combination of directions and motions that produced them, the result is a phase rotation of the spin-echo signals derived from volume elements within the region of interest.

In hybrid space, the difference in I, Q values at a point with the same x coordinate as the object for the static and moving cases simply represents a phase shift $\Delta\phi_p = \Delta\phi_{pk}$ (Eq A11), where the subscript k implies that the phase shift would depend on the specific motion at the time of each spin echo. If such instantaneous phase shift data could be obtained, then

the effects of global intraview motion could be adaptively removed from an image data set simply by applying the appropriate reverse phase rotation. Note that this would not remove the effect of intravoxel phase dispersion (vascular structures primarily). As with previous corrections, the corrective phase shifts can be applied in hybrid space or data space.

Combined corrections.—It is possible to combine all of these operations so that a data set can be adaptively corrected to reduce artifacts, intensity loss, and unsharpness due to view-to-view object displacements and intraview phase shifts. The combined correction is particularly simple if it is applied in data space, since the phase rotations associated with each correction can be summed together to yield a single corrective phase shift for each complex data point:

$$\tilde{\zeta}' = e^{-i\Delta\phi_c}\tilde{\zeta}, \quad (\text{A12})$$

where $\Delta\phi_c(j,k,l) = \Delta\phi_x + \Delta\phi_y + \Delta\phi_z + \Delta\phi_p$ (Eq 13) for three-dimensional Fourier transform and $\Delta\phi_c(j,k) = \Delta\phi_x + \Delta\phi_y + \Delta\phi_p$ (Eq 14) for two-dimensional Fourier transform.

APPENDIX B

The most important assumption in Appendix A is that only a single globally moving object is present within the field of view. This may be a good representation of gross body movements due to voluntary motion, but it is not satisfactory for modeling the effects of respiratory motion in the abdomen.

Implications of the "Mixture Issue"

Adaptive correction algorithms.—Consider the situation in which static and mobile objects are both present within the field of view of an MR image acquisition. If the algorithms outlined in Appendix A are applied to correct the raw data for the motion of the mobile object (thereby depicting it more clearly), then the static object will be portrayed as if it were moving as shown in Figure 8d. Similarly, in a conventional coronal MR image of the abdomen, the domes of the diaphragm, as well as the liver, kidneys, and spleen, are unsharp due to the craniocaudal reciprocation of respiratory motion. The coronally imaged spine and the lateral abdominal walls are relatively sharp. If the MR image data of such an acquisition were successfully corrected to make the mobile visceral structures appear to be static and sharp in the corrected image, then the spine and abdominal wall would appear blurred. No information is truly lost since either image could be reconstructed from the same raw data.

It is reasonable to simply decide which structures are of greatest clinical importance and then to adaptively bring these into best focus. This raises the possibility

of implementing corrections of varying magnitude to allow structures with slightly differing motions to be selectively focused on an interactive basis.

A problem might arise if a static structure such as the lateral abdominal wall begins to generate marked artifacts when an image is adaptively corrected for visceral motion. Several solutions may be possible. Since the adaptive method is completely independent of other artifact reduction techniques such as ordered phase encoding (13), it should be possible to use these in a complementary fashion. We speculate that ordered phase encoding should be helpful in the situation just described.

The second possible solution to the "mixture problem" is to apply the correction techniques only to selected vertical strips of the hybrid space data set, thereby regionally correcting for motion, as shown in Figure 8d.

A third possibility is to exploit the Fourier addition theorem. A correction could be implemented to improve the depiction of one region in an MR image. This portion of the image could then be removed and saved. A different correction could then be applied to the same raw data and the appropriate segment of the image again removed and saved. This process would be repeated several times until a satisfactory complete image is obtained. At any time when a portion of the image is removed, the remainder could be converted back into its original state by inverse transformation and reversal of the correction.

Measurement of motion with NAV echoes.—The task of measuring displacements and phase shifts becomes more challenging when combinations of mobile and static structures are present in the field of view. A variety of modifications of the approach for measuring displacement with NAV echoes are feasible. In a case in which the field of view contains discrete static and mobile objects, the cross correlation operations could be performed (in hybrid space) on only a segment of each NAV echo frame. This segment would be limited to the region of the moving object and would exclude discrete static objects. In cases in which the scene is complex, with few high contrast edges, the ability to track movements with hybrid space data might be improved by edge enhancement by means of blurred mask subtraction of the one-dimensional modulus NAV projections.

Preliminary studies of the problem of measuring phase shifts in moving structures, when static material is also present, have proved interesting. Figure B1 illustrates data from a phantom study that was similar to the one shown in Figure 5, except that a static phantom was also placed into the imaged section, parallel to the mobile phantom and the x axis. The mobile phantom was manually reciprocated in the x direction at varying velocities of up to about 5 cm/sec during acquisition, and data were collected with a sequence

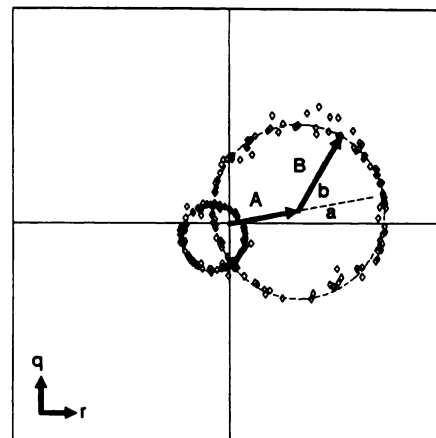


Figure B1. Phase shifts due to intraview motion (q = quadrature component of the spin echo, r = real component of the spin echo).

containing two X-NAV echoes at TEs of 30 and 72 msec.

The data points plotted in Figure B1 are complex I,Q values from a single column in the Fourier-transformed (hybrid space) X-NAV data array. Note that the pattern consists of two rings of points, with the larger ring corresponding to the first echo. If no motion were present, all of the points constituting the ring would be expected to cluster at one location in the plane. Instead, intraview phase shifts have caused the I,Q vectors to be rotated, depending on the velocity at the time of each echo. The centers of the circles are displaced from the origin because each I,Q vector is composed of a static vector A , which is due to stationary spins, and a vector B , which reflects the quantity and phase of moving spins.

In the context of the adaptive correction technique, the phase shift that must be determined in each of the NAV projections (represented by the individual I,Q points) is the angle of vector B with respect to the coordinate system, rather than the angle of $A + B$. This could be obtained by finding the center of curvature of the circle or arc of points in a given hybrid space column by a curve-fitting technique, and then subtracting the coordinates of this point from each pair of I,Q values and computing the phase of the resultant vectors. ■

References

- Schultz CL, Alfidi RJ, Nelson AD, Kopywoda SY, Clappitt ME. The effect of motion on two-dimensional Fourier transformation magnetic resonance images. *Radiology* 1984; 152:117-121.
- Ehman RL, McNamara MT, Brasch RC, Felmlee JF, Gray JE, Higgins CB. Influence of physiologic motion on the appearance of tissue in MR. *Radiology* 1986; 159:777-782.
- Axel L, Summers RM, Kressel HY, Charles C. Respiratory effects in two-dimensional Fourier transform MR imaging. *Radiology* 1986; 160:795-801.
- Wood ML, Henkelman RM. Magnetic field dependence of the breathing artifact. *Magn Reson Imaging* 1986; 4:387-392.

5. Wood ML, Henkelman RM. Suppression of respiratory motion artifacts in magnetic resonance imaging. *Med Phys* 1986; 13: 794-805.
6. Frahm J, Haase A, Matthaei D. Rapid NMR imaging of dynamic processes using the FLASH technique. *Magn Reson Med* 1986; 3:321-327.
7. Paling MR, Brookeman JR. Respiration artifacts in MR imaging: reduction by breath holding. *J Comput Assist Tomogr* 1985; 10:1080-1082.
8. Unger EC, Cohen MS, Gatenby RA, et al. Single breath-holding scans of the abdomen using FISP and FLASH at 1.5 T. *J Comput Assist Tomogr* 1988; 12:575-583.
9. Rzedzian RR, Pykett IL. Instant images of the human heart using a new, whole-body MR imaging system. *AJR* 1986; 149:245-250.
10. Stark DD, Hendrick RE, Hahn PF, Ferrucci JT Jr. Motion artifact reduction with fast spin-echo imaging. *Radiology* 1987; 164: 183-191.
11. Lanzer P, Botvinick EH, Schiller NB, et al. Cardiac imaging using gated magnetic resonance. *Radiology* 1984; 150:121-127.
12. Ehman RL, McNamara MT, Pallack M, Hricak H, Higgins CB. Magnetic resonance imaging with respiratory gating: techniques and advantages. *AJR* 1984; 143:1175-1182.
13. Bailes DR, Gilderdale DJ, Bydder GM, et al. Respiratory ordered phase encoding (ROPE): method for reducing respiratory motion artifacts in MR imaging. *J Comput Assist Tomogr* 1985; 9:835-838.
14. Pattany PM, Phillips JJ, Chiu LC, et al. Motion artifact suppression technique (MAST) for MR imaging. *J Comput Assist Tomogr* 1987; 11:369-377.
15. Felmlee JP, Ehman RL. Spatial presaturation: a method for suppressing flow artifacts and improving depiction of vascular anatomy in MR imaging. *Radiology* 1987; 164:559-564.
16. Edelman RR, Atkinson DJ, Silver MS, Loaiza FL, Warren WS. FRODO pulse sequences: a new means of eliminating motion, flow, and wraparound artifacts. *Radiology* 1988; 166:231-236.
17. Haacke EM, Patrick JL. Reducing motion artifacts in two-dimensional Fourier transform imaging. *Magn Reson Imaging* 1986; 4:359-376.
18. Suramo L, Paivansalo M, Myllyla V. Craniocaudal movements of the liver, pancreas, and kidneys in respiration. *Acta Radiol* 1984; 25:129-131.
19. Hinks RS. Monitored echo gating (MEGA) for the reduction of motion artifacts (abstr). *Magn Reson Imaging* 1988; 6(suppl 1):48.
20. Bracewell RN. The Fourier transform and its applications. 2nd ed. New York: McGraw-Hill, 1978; 104.
21. Carr HY, Purcell EM. Effects of diffusion on free precession in nuclear magnetic resonance experiments. *Phys Rev* 1954; 94:630-638.
22. Moran PR, Moran RA, Karstaedt N. Verification and evaluation of internal flow and motion: true magnetic resonance imaging by the phase gradient modulation method. *Radiology* 1985; 154:433-441.
23. Van Dijk P. Direct NMR imaging of heart wall and blood flow velocity. *J Comput Assist Tomogr* 1984; 8:429-436.
24. von Schulthess GK, Higgins CB. Blood flow imaging with MR: spin-phase phenomena. *Radiology* 1985; 157:687-695.
25. Axel L. Blood flow effects in magnetic resonance imaging. *AJR* 1984; 143:1157-1166.
26. Bradley WG Jr, Waluch V. Blood flow: magnetic resonance imaging. *Radiology* 1985; 154:443-450.